Subcritical Kelvin-Helmholtz Instability in a Hele-Shaw Cell

L. Meignin, P. Gondret, C. Ruyer-Quil, and M. Rabaud

*Laboratoire Fluides, Automatique et Systèmes Thermiques, Universités Paris-Sud and P. & M. Curie, and CNRS (UMR 7608),
Bâtiment 502, Campus Universitaire, 91405 Orsay Cedex, France*

We investigate experimentally the subcritical behavior of the Kelvin-Helmholtz instability for a
gas-liquid shearing flow in a Hele-Shaw cell. The subcritical curve separating the solutions of a stable
plane interface and a fully saturated nonlinear wave train is determined. Experimental results are
fitted by a fifth order complex Ginzburg-Landau equation whose linear coefficients are compared to
theoretical ones.

Wave formation by wind blowing over the sea is a puzzling phenomenon that has attracted the attention of physicists for many decades. In 1871, Lord Kelvin made the linear stability analysis of two inviscid fluid layers in relative shearing motion by using what is now known as the method of normal modes [1]. It was the first time this method was used in the context of hydrodynamic stability. The "Kelvin-Helmholtz (KH) mechanism" responsible for the instability relies on a pressure gradient in phase with the wave crests being sufficiently large to overcome the restoring forces of gravity and surface tension. The experiments of Thorpe in 1969 [2] have demonstrated that in the case of two liquids of weak density contrast the inviscid model is applicable to real flows, where boundary layers are necessarily present at the interface. Kelvin himself recognized that his model strongly overestimates the onset of waves when the wind flows over a body of water. More sophisticated models involving air turbulence modeling, drift of the interface, as well as spatial evolution of the wind force (the "fetch") are still not completely satisfying [3]. The nonlinear analysis of Weissman in 1979 [4] shows that the KH instability becomes subcritical for fluids of large enough density contrast.

Here we investigate experimentally the KH instability with a gas to liquid density ratio of order 10^{-3}, much smaller than the critical value 0.283 predicted by Weissman [4] for the instability to be subcritical. The experiment was performed in a particular well controlled geometry: a Hele-Shaw cell consisting of two glass plates separated by a small gap where the two fluids flow parallel (Fig. 1). In such a setup, below the instability threshold, the flow is governed by Darcy's law: the flow remains laminar, two dimensional, steady, and uniform [5]. Above the threshold, interfacial waves form and propagate. The linear regime was studied both experimentally and analytically [6–8]: If the growth rate and the phase velocity of the waves are both controlled by the wall friction, the onset of the instability is found to be very close to the inviscid KH prediction. Furthermore, as it is an open flow, a transition between a convective (*C*) and an absolute (*A*) regime has been predicted analytically and

observed experimentally [9]. The *C/A* transition was found experimentally to be nonlinear with typical scaling laws [10]. In this Letter we show that the first bifurcation leading to the wave formation is subcritical, i.e., that the threshold of wave formation increases as the noise amplitude decreases. To our knowledge, the complete measurement of the subcritical instability curve for an open convective flow has never been reported. Our result may thus be a key step for a better understanding of sea wave formation.

The experimental cell is made of two glass plates a distance $b = 0.35$ mm apart and placed horizontally on the edge so that gravity acts parallel to the cell and perpendicular to the gas-liquid interface. The two fluids are nitrogen (density $\rho_g = 1.28$ kg m^{-3}, viscosity $\eta_g = 1.75 \times 10^{-5}$ Pa s) and silicon oil ($\rho_l = 952$ kg m^{-3}, $\eta_l = 2.0 \times 10^{-2}$ Pa s) with corresponding interfacial tension $\gamma = 20 \times 10^{-3}$ N/m. Both fluids enter the cell at the same pressure and flow out at atmospheric pressure. The injection pressure is measured with a feedback loop that ensures a relative precision of 10^{-3}. The basic laminar flow is governed by Darcy's law so that the gap averaged velocities $\overline{U}_g$ and $\overline{U}_l$ are linked to the fluid viscosities η_g and η_l by the relation $\overline{U}_g = (\eta_l/\eta_g)\overline{U}_l$. As the viscosity ratio is of the order of 10^3, typical velocities are $\overline{U}_l \sim 5$ mm/s $\ll \overline{U}_g \sim 5$ m/s. In the following, we drop the bar notation and use the gas velocity U_g as the control parameter. By a small periodic modulation of the oil injection pressure a sinusoidal interface deformation of controlled amplitude A_0 and frequency f can be imposed at the end of the splitter tongue where the two fluids meet. The interface is observed perpendicular to the glass plates
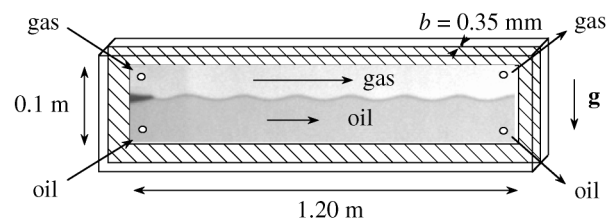

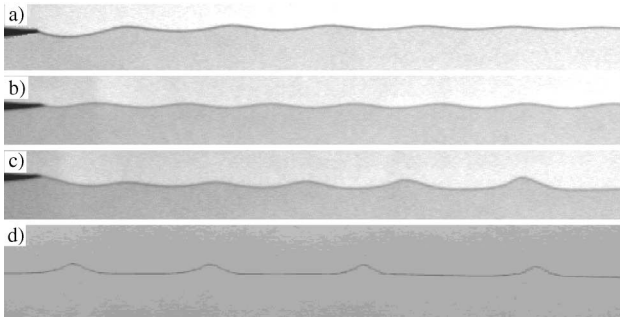FIG. 1. Sketch of the experimental setup.

FIG. 2. Spatial evolution of the interface over the first 7 cm downstream when a sinusoidal perturbation of amplitude $A_0 = 2$ mm and frequency $f = 0.4$ Hz is imposed at the inlet: (a) below onset, (b) at onset, and (c) just above onset. (d) Saturated cnoidal waves far downstream.

by a video charged-coupled device camera. For more details on the experimental setup, see Refs. [6,9,11,12].

When U_g is small enough, the interface remains stable and horizontal. At larger U_g, the interface modulation at inlet of controlled amplitude A_0 is either damped [Fig. 2(a)], or marginal [Fig. 2(b)], or amplified downward [Fig. 2(c)] depending upon the value of U_g and upon the forcing frequency f. The waves created remain sinusoidal over the first few centimeters with wavelength $\lambda \sim 1$ cm. When amplified they rapidly turn to a nonlinear shape and appear to propagate as cnoidal waves with the saturated amplitude $A_{sat} \sim 3$ mm and a wavelength of a few centimeters [Fig. 2(d)].

The study of the instability threshold as a function of the forcing frequency f allows us to build the marginal stability curve of the system for a given forcing amplitude A_0 (Fig. 3). This curve is parabolic in shape and the instability threshold which corresponds to the minimum of the curve is here $U_{gc} = 4.5$ m/s for the critical frequency $f_c = 0.4$ Hz. For each point of the marginal curve, the wave number is measured and is used in the following. Note that when the forcing amplitude is varied, the instability threshold varies but the parabolic shape of the marginal stability curve remains.
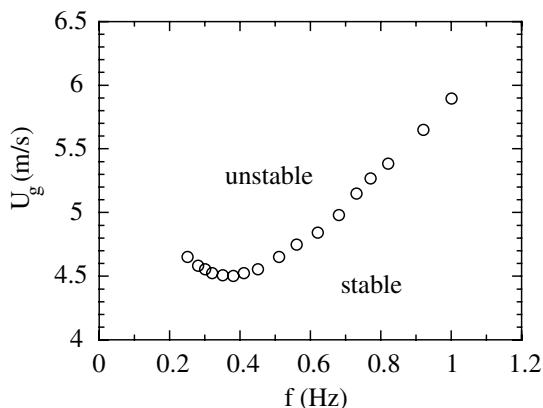

FIG. 3. Experimental marginal stability curve U_g vs f obtained at the forcing amplitude $A_0 \sim 0.6$ mm.

We study the instability threshold U_{gc} for different forcing amplitude A_0 at the most unstable frequency f_c. It appears that U_{gc} is a decreasing function of A_0. Indeed, for small values of U_g, the system relaxes downstream to the plane stable interface whatever the A_0 value. By contrast, for U_{gc} values around 4.5 m/s, we found a critical forcing amplitude below which the perturbations relax to zero, but above which the perturbations are spatially amplified and take ultimately the cnoidal shape of Fig. 2(d) with the amplitude A_{sat}. We can thus draw the separatrix between the two attractor domains, namely, the horizontal interface and the saturated cnoidal wave train (Fig. 4). For $A_0 > A_{sat}$, the interface relaxes downstream to the cnoidal wave train if $U_g \geq 4.21$ m/s. All these findings demonstrate the subcritical nature of the transition with the bistability domain $4.21 \leq U_g \leq 4.63$ m/s. The bifurcation diagram of Fig. 4 is obtained either by a periodic forcing or by an impulsive forcing. An adjustment by a fifth order Landau equation is in rather good agreement with the measurements and gives the onset of the instability at $U_{gc} = 4.63$ m/s. Varying the gap thickness in the range 0.175 mm $< b < 0.800$ mm, the instability remains subcritical.

Note that the instability is first convective: The response of the interface to an impulsive perturbation is the formation of a wave packet that spreads but is advected downstream. The rear front velocity V_f of the wave packet decreases when U_g increases up to the C/A transition observed for $U_{ga} > U_{gc}$ [9]. In the absolute regime, self-sustained waves are observed at the interface downstream of a healing length that decreases when U_g increases.

Let us now characterize the subcritical bifurcation between the flat interface and the convectively unstable
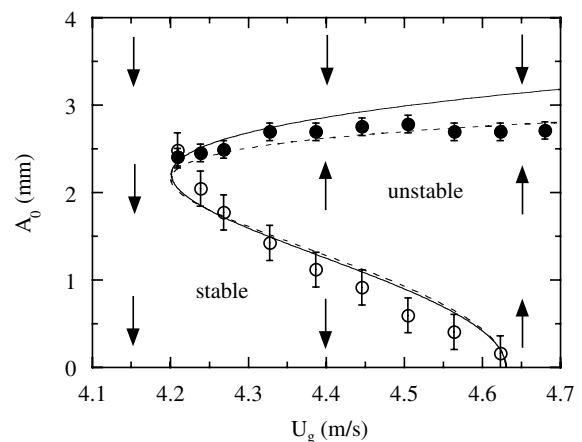

FIG. 4. Bifurcation diagram A_0 vs U_g: (○) limit between spatially amplified or damped waves, (●) amplitude of the downstream saturated waves, (—) fit by a fifth order Landau equation ($g = 3.8 \times 10^{-2}$ mm^{-2} and $h = 3.9 \times 10^{-3}$ mm^{-4}), (- - -) fit by a modified Landau equation with $g = 3.5 \times 10^{-2}$ mm^{-2}, $h = 2.8 \times 10^{-3}$ mm^{-4}, $A_{sat} = 3.5$ mm, and $n = 4$.

wavy state by a complex Ginzburg-Landau (CGL) equation of order 5. Considering the evolution of a slowly modulated wave such that the interface position can be described by the real part of $A(x, t) \exp[i(k_c x - \omega_c t)]$, where k_c and ω_c refer, respectively, to critical wave number and frequency at threshold, this equation classically reads in 1D form [13]

$$\tau_0 \left[\frac{\partial A}{\partial t} + V_g \frac{\partial A}{\partial x} \right] = \mu(1 + ic_0)A + \xi_0^2(1 + ic_1)\frac{\partial^2 A}{\partial x^2}$$
$$+ g(1 + ic_2)|A|^2 A - h|A|^4 A, \qquad (1)$$

where x denotes the flow direction and $\mu = (U_g - U_{gc})/U_{gc}$ is the reduced control parameter. The six coef-

ficients τ_0, V_g, c_0, ξ_0, c_1, c_2 are real, and g and h are also assumed to be real. The choice of the nonlinear terms is the result of the translational symmetry which implies that a solution remains invariant through any phase shift. As usual, only the simplest quintic term ensuring the amplitude saturation is kept.

If we restrict ourselves to the case of monochromatic waves close to threshold such as $A(x, t) = A_0 \exp[i(k - k_c)x - i(\omega - \omega_c)t]$ with real ω and complex $k = k_r + ik_i$ corresponding to the experimental configuration, Eq. (1) yields a system of two equations (the real and complex parts) [14]:

$$-\tau_0 V_g k_i = 2k_i(k_r - k_c)\xi_0^2 c_1 + \mu - \xi_0^2[(k_r - k_c)^2 - k_i^2]$$
$$+ g|A|^2 - h|A|^4, \qquad (2)$$

$$\tau_0[-(\omega - \omega_c) + V_g(k_r - k_c)] = \mu c_0 - \xi_0^2 c_1[(k_r - k_c)^2 - k_i^2] + gc_2|A|^2 - 2\xi_0^2 k_i(k_r - k_c). \qquad (3)$$

Each of the eight coefficients can be determined from the experiments by considering some particular cases which cancel terms in Eqs. (2) and (3) as follows.

The experimental subcritical curve (Fig. 4) corresponds to Eq. (2) for $k_r = k_c$ (forcing at the critical mode) and $k_i = 0$ (marginal state) which thus reduces to the fifth order Landau equation $\mu + gA_0^2 - hA_0^4 = 0$ for small A_0. The corresponding fit of Fig. 4, which gives $g = (3.8 \pm 0.6) \times 10^{-2}$ mm^{-2} and $h = (3.9 \pm 1.3) \times 10^{-3}$ mm^{-4}, is not completely satisfying as it does not mimic the strong experimental saturation. This deviation is due to the strong nonharmonic shape of the saturated cnoidal waves. A better agreement can be obtained by replacing h by $h/[1 - (|A|/A_{\text{sat}})^n]$ (see Fig. 4 with $A_{\text{sat}} = 3.5$ mm and $n = 4$), a compact expression for taking into account terms of order higher than 5 [15].

The experimental marginal stability curve (Fig. 3) corresponds again to Eq. (2) for $k_i = 0$ (marginal state) but now close to the critical mode k_c and Eq. (2) thus now reduces for small A to $\mu - \xi_0^2(k_r - k_c)^2 = 0$. The experimental data fit leads to $\xi_0 = (0.90 \pm 0.02)$ mm, meaning that the coherence length ξ_0 is quite small, roughly a tenth of the wavelength.

The coefficient V_g can be determined from the evolution of the rear front velocity V_f with U_g in the convectively unstable regime. Indeed, considering the CGL equation in the linear regime, one obtains [16] $V_f = V_g - (2\xi_0/\tau_0)\sqrt{(1 + c_1^2)\mu}$. The fit of the experimental data $V_f = f(\mu)$ leads to $V_g = (4.0 \pm 0.3)$ mm/s and $\sqrt{1 + c_1^2}/\tau_0 = (2.7 \pm 0.3)$ s^{-1}. τ_0 is determined by measuring the spatial growth rate k_i just above onset at the critical mode k_c. For that we measure the amplitude evolution $A(x)$ of the waves downstream for the smallest forcing amplitude A_0 at different U_g values. Indeed, Eq. (2) for $k_r = k_c$ and small $|A|$ reduces to $-\tau_0 V_g k_i = \mu + \xi_0^2 k_i^2$. Fitting the experimental data $k_i(\mu)$ with

the known V_g value, we obtain $\tau_0 = 0.57 \pm 0.05$ s. With the $\sqrt{1 + c_1^2}/\tau_0$ value found above, we then deduce $|c_1| = 1.2 \pm 0.5$.

For the determination of the last two coefficients, c_0 and c_2, we use Eq. (3) at the marginal state ($k_i = 0$, $|A| = A_0$): $\tau_0[-(\omega - \omega_c) + V_g(k_r - k_c)] = \mu c_o - \xi_0^2 c_1[(k_r - k_c)^2] + gc_2 A_0^2$. For a given forcing amplitude (here $A_0 = 1$ mm), we measure k_r for different imposed values of μ and ω. As the other coefficients are now known, we obtain for each pair of values (μ, ω) an equation relating c_0 and c_2. We found the best fit for $c_0 = -0.14 \pm 0.07$ and $c_2 = 0.65 \pm 0.25$. This allows us to check that $c_1 > 0$ so that $c_1 = +1.2 \pm 0.5$.

Thus we have been able to determine all eight CGL coefficients. However, the CGL equation requires that the amplitude of the nonlinear terms is small, while strong nonlinear effects are observed in the experiments. This may explain the bad precision obtained for some coefficients, e.g., c_2, which is related to the variation of the frequency ω with the amplitude A.

All the experimentally determined coefficients τ_0, V_g, c_0, ξ_0, c_1, which describe the linear behavior, can be compared to their theoretical values that can be extracted from the dispersion relation $\omega(k)$ of the linear stability analysis of Ref. [6] improved in [7]. In the limiting gas/liquid case of low density and viscosity ratio (ρ_g/ρ_l, $\eta_g/\eta_l \ll 1$) corresponding to the experimental configuration, the dispersion relation takes the form

$$\omega = 2\frac{\eta_g}{\eta_l}U_g k_r + i\frac{b^2 k_r^2}{10\eta_l}\left[\frac{9}{7}\rho_g U_g^2 - \frac{5}{6}\frac{(\rho_l g + \gamma\frac{\pi}{4}k_r^2)}{k_r}\right]. \qquad (4)$$

The analytical expression of the theoretical linear CGL coefficients, together with their numerical values considering the experimental physical parameter values, are

234502-3   234502-3

thus [17]

$$V_g = 2\frac{\eta_g}{\eta_l}U_{gc} = 6.1 \text{ mm/s}, \tag{5}$$

$$\xi_0 = \frac{1}{2k_c} = 0.65 \text{ mm}, \tag{6}$$

$$\tau_0 = \frac{70}{9}\frac{1}{\text{Re}_c\omega_c} = 0.07 \text{ s}, \tag{7}$$

$$c_0 = -\frac{70}{9}\frac{1}{\text{Re}_c} = -0.33, \tag{8}$$

$$c_1 = 0. \tag{9}$$

In the above analytical expressions, $U_{gc} = (35/54\rho_g)^{1/2}(\pi\gamma\rho_l g)^{1/4} = 3.5$ m/s is the instability threshold, $k_c = (4\rho_l g/\pi\gamma)^{1/2} = 771$ m^{-1} is the critical wave number calculated with the effective surface tension $\gamma^* = \pi\gamma/4$, for taking into account the principal radii of curvature across the gap for a liquid that is perfectly wetting, $\omega_c = V_g k_c = 4.7$ s^{-1} is the critical frequency, and $\text{Re}_c = \rho_g U_{gc}k_c b^2/\eta_g = 24$ is the critical gas reduced Reynolds number.

The coefficient V_g is found to be equal to the phase wave velocity at onset (as in the classical KH instability), which is here twice the liquid velocity and its theoretical value is in quite good agreement with the experimental value. The coefficient ξ_0 corresponds to half the capillary length $l_c = 1/k_c$ and its theoretical value is also in quite good agreement with the experimental value. The time coefficient τ_0 is related to the inverse of the critical frequency ω_c. The theoretical value of τ_0 is quite far from its experimental value, but this is consistent with the fact that the measured growth rate is found to be quite different from its theoretical values [11]. The coefficient c_0 is inversely proportional to the critical gas Reynolds number and its theoretical value is in rather good agreement with the experimental value. The coefficient c_1 is strictly zero in the theoretical analysis but nonzero in the experimental findings even if quite weak. One possible reason for all these disagreements is that the analytical dispersion relation has been derived from a two-dimensional model obtained by averaging the fluid velocity across the gap of the cell. But following the recent tridimensional approach to the problem [8], we found coefficient values close to the 2D model except for c_1 which is now strictly positive [18], so much closer to the experimental value.

To our knowledge, this experiment is the first that allows for a complete determination of the subcritical bifurcation curve in a open flow configuration, even if a hysteresis of the onset has been observed recently in two-dimensional wakes [19,20]. The numerical simu-lation of a quintic CGL equation with the experimentally determined coefficients should bring interesting points of comparison with the rich dynamics of the observed waves, in particular, the occurrence of secondary instabilities such as the Eckhaus or Benjamin-Feir mechanism [21].

Going back to the sea wave formation, even if turbulence makes the real problem much more complex, the subcritical behavior of the KH instability shown here may partly explain why classical linear analysis of the onset value overestimates the observed wind force as already noted by Kelvin.

[1] Lord Kelvin, Philos. Mag. **42**, 362–377 (1871).
[2] S. A. Thorpe, J. Fluid Mech. **39**, 25 (1969).
[3] F. Veron and W. K. Melville, J. Fluid Mech. **446**, 25–65 (2001).
[4] M. A. Weissman, Philos. Trans. R. Soc. London A **290**, 639 (1979).
[5] P. Gondret *et al.*, Phys. Fluids **9**, 1841 (1997).
[6] P. Gondret and M. Rabaud, Phys. Fluids **9**, 3267 (1997).
[7] C. Ruyer-Quil, C. R. Acad. Sci., Ser. IIb: Mec., Phys., Chim., Astron. **329**, 337 (2001).
[8] F. Plouraboué and E. J. Hinch, Phys. Fluids **14**, 922 (2002).
[9] P. Gondret *et al.*, Phys. Rev. Lett. **82**, 1442 (1999).
[10] J.-M. Chomaz and A. Couairon, Phys. Fluids **11**, 2977 (1999).
[11] L. Meignin *et al.*, Phys. Rev. E **64**, 026308 (2001).
[12] L. Meignin, Ph.D. thesis, Université Paris-Sud, 2001.
[13] P. Kolodner, Phys. Rev. A **46**, 6431 (1992).
[14] V. Croquette and H. Williams, Phys. Rev. A **39**, 2765 (1989).
[15] St. Hollinger, P. Büchel, and M. Lücke, Phys. Rev. Lett. **78**, 235 (1997).
[16] H. W. Müller, M. Lücke, and M. Kamps, Europhys. Lett. **10**, 451 (1989).
[17] The coefficients of the linear part of the CGL equation are related to the partial derivatives of the frequency ω relative to the wave number k and the control parameter U_g at the onset (k_c, U_{gc}) by the relations [A. Tsameret and V. Steinberg, Phys. Rev. E **49**, 1291 (1994)]:
$V_g = \text{Re}[\frac{\partial\omega}{\partial k_r}|_c]$,
$\xi_0^2 = -\text{Im}[\frac{\partial^2\omega}{\partial k_r^2}|_c]/(2U_{gc}\text{Im}[\frac{\partial\omega}{\partial U_g}|_c])$,
$\tau_0 = 1/(U_{gc}\text{Im}[\frac{\partial\omega}{\partial U_g}|_c])$,
$c_0 = -\text{Re}[\frac{\partial\omega}{\partial U_g}|_c]/\text{Im}[\frac{\partial\omega}{\partial U_g}|_c]$,
$c_1 = -\text{Re}[\frac{\partial^2\omega}{\partial k_r^2}|_c]/\text{Im}[\frac{\partial^2\omega}{\partial k_r^2}|_c]$.
[18] From the 3D theoretical analysis of [8], we found $V_g = 8.3$ mm/s, $\xi_0 = 0.71$ mm, $\tau_0 = 0.076$ s, $c_0 = -0.47$, and $c_1 = 0.37$ with $U_{gc} = 3.55$ m/s and $k_c = 738$ m^{-1}.
[19] J. Zhang *et al.*, Nature (London) **408**, 835 (2000).
[20] V. K. Horváth *et al.*, Phys. Rev. E **61**, R4702 (2000).
[21] L. Ning and R. E. Ecke, Phys. Rev. E **47**, 3326 (1993).